A new scheme for retrieving ocean surface salinity from simulated multi-angular SMOS brightness temperature

WANG Zhen-zhan，YIN Xiao-bin

(*Center for Space Science and Applied Research*，*CAS*，*Beijing* 100190，*China*)

Abstract: The European Space Agency will launch the first salinity satellite for remotely sensing the global soil moisture and ocean salinity (SMOS) at a sun-synchronous orbit in 2009. One of the payloads on the satellite is a synthetic aperture microwave radiometer (MIRAS)，which is an innovative instrument designed as a two-dimensional (2D) interferometer for acquiring brightness temperature (T_B) at L-band (1.4 GHz). MIRAS allows measuring T_B at a series of incidences for full polarizations. As the satellite travels，a given location within the 2D field of view is observed from different incidence angles.

The authors develop a new scheme to retrieve the sea-surface salinity (SSS) from SMOS's T_B at multi-incidence angles in a pixel，utilizing the properties of emissivity changing with incidence angles. All measurements of a given Stokes parameter in a pixel are first fitted to incidence angles in three order polynomial，and then the smoothed data are used for retrieving the SSS. The procedure will remove the random noise in T_B greatly.

Furthermore，the new method shows that the error in retrieved SSS is very sensitive to the system biases in the calibrated T_B of the sensor，but the error in the retrieval is also a system bias，which can be corrected by post-launch validation. Therefore，this method may also serve as a means to evaluate the calibration precision in T_B.

Key words: SMOS；salinity retrieval；multi-incidence angle

CLC number: TP79；P731 **Document code:** A **Serial number:** 1009-5470(2009)05-0011-07

1 Introduction

Both soil moisture and ocean salinity are important variables for weather，climate，and extreme-event forecasting. The European Space Agency's Soil Moisture and Ocean Salinity (SMOS) satellite，which is scheduled for launch in 2009，will be equipped with a synthetic aperture microwave radiometer (MIRAS) instrument，an innovative 2-D synthetic aperture interferometer at L-band[1,2]，to estimate the sea surface salinity (SSS) with an accuracy of 0.1–0.2 per salinity unit(psu)when retrievals are averaged over a 10–30 day period and over an open ocean area of 200 km ×200 km[3]，as required by the Global Ocean Data Assimilation Experiment (GODAE). Such accuracy is also required to realize the scientific targets in global water cycles and environment changes[4].

As part of the preparation of the Level-2 ground segment processing for the SMOS mission，a salinity retrieval algorithm is implemented in the Level-2 Salinity Prototype Processor (L2SPP)[5]. The algorithm is based on an iterative inversion method that compares the brightness temperature (T_B) reconstructed from the measured visibilities at different incidence angles with the T_B simulated by a full forward model[6].

Because the sensitivity of SMOS signal in a single measurement will generally increase from 0.2 K at the center to 3.0 K at the edges of the swatch，theoretically a single observation cannot retrieve SSS with an accuracy of 0.1–0.2 psu. In order to meet the requirement to the accuracy of the retrieval，there usually are two kinds of method to retrieve SSS from SMOS measurements. One is to try to improve the salinity accuracy by averaging all the retrieved SSS from a set of T_B measurements at a given incidence angle；another is first to average all possible measurements at the same angle and then to retrieve SSS using the averaged T_B in order to reduce the noise in the measure-

Received date: 2008-12-13； **Revised date:** 2009-03-02. Editor：SUN Shu-jie

Fundation item: State 863 Program(2009AA09Z102)

Biography: WANG Zhen-zhan，born in Dec. 1969 and received Ph.D in Aug. 2005 in polarimetric microwave remote sensing oceanic wind vector-principle，system design and application. His major interest is in passive microwave remote sensing of ocean，land，and atmosphere，eps. in retrieval algorithm development，sensor calibration/validation，and microwave transfer model in the ocean surface and atmosphere.

ment. Both methods suffer the problem that the noise in a single observation could not be removed completely. Furthermore, received oceanic T_B is changing, since instrument noises and ocean state vary spatially differently with time, so the averaged T_B may lose the real variation in the ocean-atmosphere parameters reflected in T_B.

In the paper, a new retrieval scheme is developed to obtain SSS from SMOS T_B, i.e., using both vertical and horizontal brightness temperatures (T_{Bv} and T_{Bh}) of 1.4 GHz at multi-incidence angles in a pixel. The scheme utilizes the property of ocean emissivity changing with incidence angles at any given frequency.

Section 2 describes the multi-angular imaging of SMOS. In Section 3, we present the methodology to simulate multi-angular SMOS T_B and a new scheme to retrieve SSS from the simulated T_B. In section 4, a series of tests are presented in order to assess the performance of the algorithm. Finally, conclusions and perspectives are given for the readers.

2 Multi-angular imaging of SMOS

MIRAS applies an aperture synthesis technique to obtain high spatial resolution over a large swath, which is similar to the way of the Earth rotation synthesis in radio astronomy used to gain angular resolution. The MIRAS L-band radiometer is dual polarized (with an optional fully polarimetric mode), and it has, by virtue of the aperture synthesis and wide field of view (FOV), a multi-angular imaging capability[7]. Due to the motion of the platform, each pixel is measured several times with different spatial and radiometric resolutions and incidence angles. As shown in Fig. 1, any pixel on the Earth's surface is observed at different incidences and azimuth angles with different spatial resolutions.

The SMOS synthetic antenna consists of 69 antenna elements distributed along three equally spaced arms, resulting in a planar Y-shaped structure. Discrete samples of the complex visibility functions are obtained from the cross correlations between simultaneous signals obtained from pairs of antenna elements. The image reconstruction process computes a T_B field consistent with this discrete visibility function. The T_B field and the visibility function are related by a discrete form of an integral relationship that is somewhat analogous to a Fourier transform[8]. The SMOS measurements are affected by strong radiometric noises. It depends not only on the incidence angle but also on the across-track distance, as shown by Fig.3 in [9]. To reduce the impact of random errors, it is necessary to spatially and temporally average the parameters obtained from SMOS retrievals (each of which is derived from measurements obtained from multiple views of a given area on Earth (i.e., a "footprint"), where each measurement corresponds to a footprint on the order of 40–50 km in diameter in order to reduce the noise of the retrieved parameters[10,11].

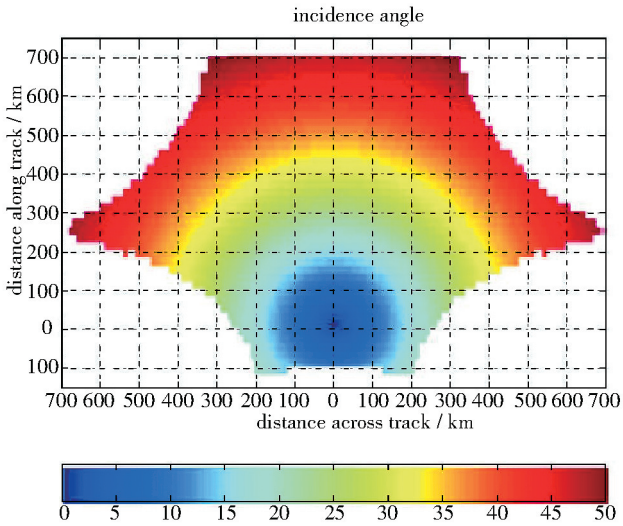

Fig.1 Typical MIRAS alias-free FOV, ground incidence angle, and pixel size represented in ground coordinates[7]

During a satellite overpass, however, numerous measurements are acquired at the same location on the Earth's surface, resulting in nearly collocated (on the Earth) measurements with incidence angles ranging from 0° at nadir to approximately 55° at the edge of the swath. This capability can be exploited to reduce the impact of radiometric noise on salinity retrieval.

3 Geophysical parameter retrieval algorithms

3.1 Simulation of SMOS brightness temperature

T_B measured at L-band not only depends on SSS but also on sea-surface temperature (SST), wind speed (WS) and atmosphere condition, because SST and SSS influence the dielectric constant of sea water, while WS is related to surface roughness.

Retrieving method begins with simulating L-band T_B at incidence angles from 0° to 55° by atmospheric millimeter propagation model (MPM)[12] and fast ocean emissivity model (FASTEM3)[13] from 2324 no-rain (liquid water content $L \leqslant 0.2$ mm) profiles of reference geophysical parameters distributed by EUMETSAT/ECMWF SAF program[14]. The database includes global atmospheric profiles on ocean surface and sea-surface parameters of each site, which represent all possible ocean states and atmosphere conditions. To avoid geographically correlated errors, an independent data set of SSS with a mean of 35 psu and root mean square (RMS) of 5 psu was added to the profiles (see [15] for an impact study of potential correlations if this effect is not taken into account). FASTEM3 in RTTOV8.5 software developed by EUMETSAT Satellite Application Facility on Numerical Weather Prediction is used to simulate ocean-surface emissivity and reflectivity of L-band.

The emissivity model can compute all four Stokes parameters of ocean microwave radiation. Because in real measurements of SMOS there are instrumental and reconstruction errors, which increase with the incidence angles, we add Gauss random noises to the simulated T_B to test our retrieving method, as shown in Fig.2. We independently simulate the noises for H (horizontal) and V (vertical) polarizations at different incidence angles. The RMS of the added Gauss random noises is 0.2K at incidence angle of 0°, and increases to 3K at 55°. These noisy T_B represent the SMOS measurements and are used to retrieve SSS with our inverse algorithms.

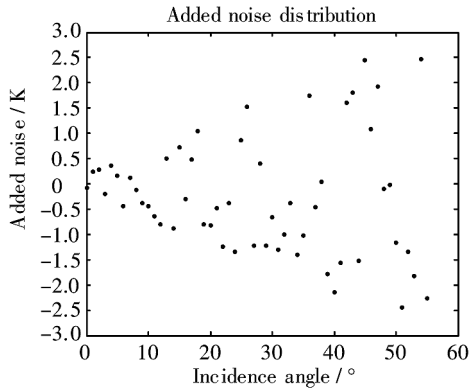

Fig.2 An example of added Gauss noise to the simulated T_B in each incidence angle at a given pixel

3.2 Retrieval algorithm

Ocean brightness temperature T_B received by SMOS can be modeled as,

$$T_B = T_{BU} + \tau\ [T_{BS} + r(T_{BD} + \tau T_{BC})], \quad (1)$$

where, T_{BU} and T_{BD} are the upwelling and downwelling atmospheric brightness temperatures, respectively. T_{BS} is sea-surface emitted brightness temperature and $T_{BS} = e \cdot T_S$, where e is sea-surface emissivity, and T_S is SST. T_{BC} is cosmic background temperature and $T_{BC} = 2.7$ K, r is ocean surface reflectivity, and τ is atmospheric transmittivity of the whole atmospheric path.

According to Peichl et al.[16], rain in the atmosphere produces a non-negligible radiative contribution when the rain intensity exceeds about 10 mm·h^{-1} (at the SMOS footprint scale). Attenuation effects of rain deserve further study, so it is not discussed here.

There are three atmospheric components to be considered for non-raining atmosphere: dry atmosphere, water vapor, and clouds. Ideally, each of the quantities identified in (1), i.e., τ, T_{BU} and T_{BD}, is the sum of the three component contributions. Our numerical simulations using the MPM model[11] show that at L-band the differences between T_{BU} and T_{BD} are less than 0.1 K. For the purpose of SMOS SSS inversion, the line-by-line model (such as MPM) is not necessary to simulate the atmospheric effects at L-band for time-saving and operational applications; therefore, in this paper a simplified regressed algorithm of τ, T_{BU} and T_{BD} is developed as the following,

$$T_{BD} = T_{BU} = T_{AE}(1 - \tau), \quad (2)$$

where T_{AE} is atmospheric effective temperature,

$$T_{AE} = aT_S + b. \quad (3)$$

Atmospheric transmittivity τ at incidence angle θ can be represented by its nadir transmittivity τ_0 at incidence angle of 0° by,

$$\ln\tau = \sec\theta \cdot \ln\tau_0. \quad (4)$$

From simulated atmospheric radiation by MPM and the above profiles, we obtain $a = 0.6968$, and $b = 62.038$ at L-band for (3). The difference between T_B in (1) simulated with the simplified atmosphere algorithm of (2)−(4) and those simulated by line-by-line model of MPM is less than 0.05 K at the low incidence angles and less than 0.1 K at 50°.

3.3 Retrieval scheme

A two-step inversion scheme is used to retrieve SSS from the simulated T_B described in section 3.1. The first step of the SSS retrieving is polynomial curve fitting of the measured T_B, according to the incidence

angle at which T_B is measured,

$$T_{B\_p}=p_3\cdot\theta^3+p_2\cdot\theta^2+p_1\cdot\theta+p_0, \quad (5)$$

where, T_{B_p} is a set of curve-fitted brightness temperatures, p_0–p_3 are coefficients of the polynomial.

Thanks to multi-angular imaging capability, each of the ground cells is measured several times with different incidence angles. The coefficients p_0-p_3 of each ground cell in (3) could be derived by regressing multi-angular noisy T_B with their incidence angles. In the nadir and near central regions, there are more samples of T_B to obtain the coefficients p_0-p_3 than those at the edge of the swath, as indicated by Fig.1.

With the help of relationship given by (5), noises in measured T_B could be greatly removed, as indicated in Fig.3. In Fig.3, black points represent noisy T_B at 0° –55° incidence angles, circles represent regressed T_{B_p}, and lines represent original simulated T_B without noise. The interval of incidence angles in Fig.3 is 1°, which means 56 samples are used to obtain the coefficients p_0–p_3 and the regressed T_{B_p} in(5).

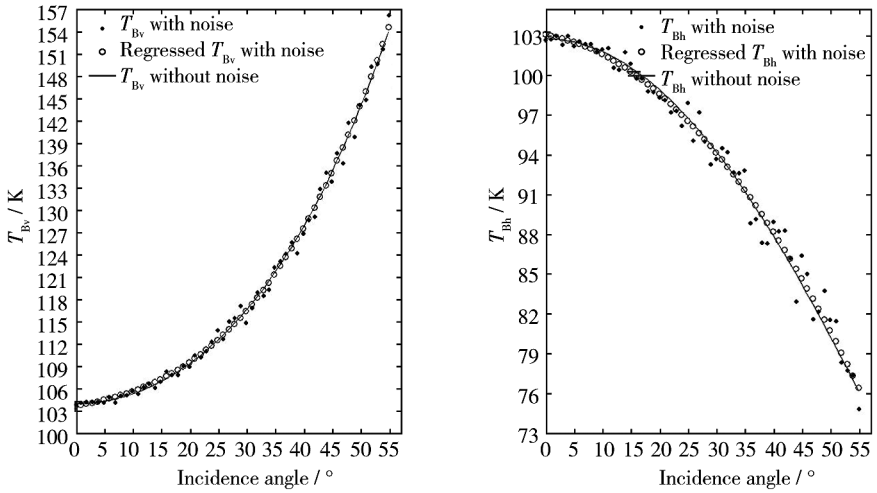

Fig.3 Comparison of noisy T_B, regressed T_{B_p} and original simulated T_B without noise

Then the Maximum Likelihood Estimation (MLE) that minimizes the differences between the regressed T_{B_p} and T_B simulated by (1) is used to inverse SSS [17]. Figure 4 illustrates the progress of retrieving SSS by the MLE. First, a guessed SSS is given, and other parameters, such as SST, WS, wind direction (WD), and τ are input using those from the given profiles. These first guessed values are adjusted to minimize a cost function. The cost function is the sum of the squared difference between the "measured" and the simulated T_B. All differences are weighted with their uncertainties, respectively. Then, the errors are obtained by taking the differences between the reference SSS and this retrieved SSS.

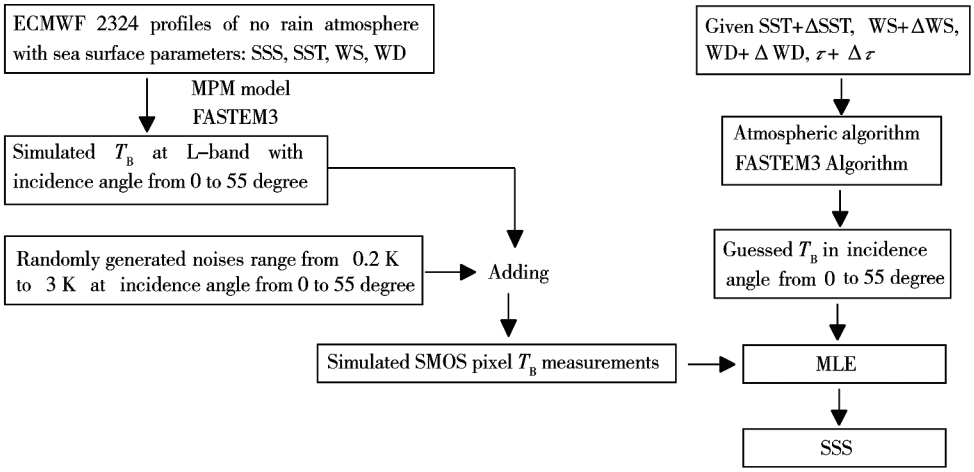

Fig.4 SSS retrieving flowchart

4 Retrieving tests

In order to evaluate the influence of the uncertainties of SST, WS, WD and τ to the SSS retrieval from the simulated T_B described in section 3.1, we add different levels of noise ΔSST, ΔWS, ΔWD, $\Delta\tau$ to the corresponding parameters. Since SMOS can measure four Stokes parameters at the same time, we may use T_{Bv} or T_{Bh} for the MLE. We may also try to use Stokes I, where I equals to T_{Bv} plus T_{Bh}, for SSS retrieving since I is not sensitive to WD.

4.1 Case 1: no error in all input parameters

We assume that there is no error in all input parameters, i.e., ΔSST=0 K, ΔWS=0 m·s^{-1}, and ΔWD=0°, and atmospheric contributions are directly calculated by applying MPM on each profile. If we denote dI for SSS RMS error of using the Stokes I to retrieve SSS, and dh for that of using T_{Bh}, and dv for T_{Bv}, we have dI=0.2 psu, dh=0.27 psu, and dv=0.25 psu. Furthermore, we find Q is not sensitive to SSS, where $Q=T_{Bv}-T_{Bh}$. The retrieved SSS using the Stokes I versus true SSS are shown in Fig. 5, whose RMS of SSS is 0.2 psu. Therefore, if there is no error in all input parameters of SSS, WS, WD, and τ, the retrieved SSS will be accurate to 0.2 psu.

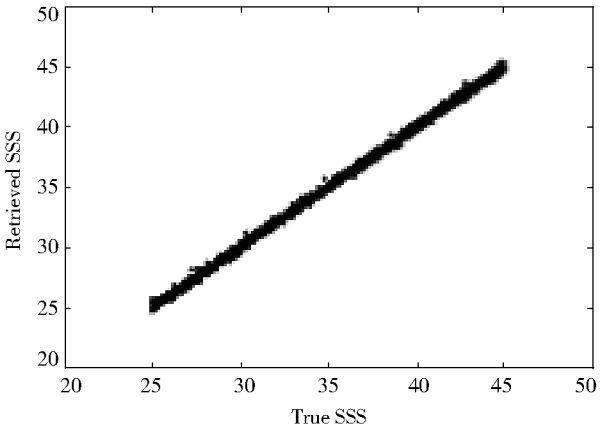

Fig.5 Retrieved SSS by Stokes I versus true SSS

4.2 Case 2: atmospheric contribution

Simplified atmospheric algorithms (2)–(4) will surely bring errors into SSS retrievals. To evaluate these errors, we use the algorithm of τ, T_{BU} and T_{BD} in (2)–(4) instead those from MPM by real profiles, which assumes that there is no error in atmospheric radiation. We find that the RMS of SSS retrievals are dI=0.19 psu, dh= 0.26 psu, and dv=0.24 psu, respectively. Therefore, the atmospheric algorithms (2)–(4) are basically accurate for SSS reversion, i.e., atmospheric algorithm errors can be ignored.

4.3 Case 3: wind direction's effects on SSS retrievals

To evaluate wind direction's effects on SSS retrievals, we set WD to be 0° for all simulations, i.e., we ignore wind direction contribution in emissivity. The results of the retrieval are dI=0.38 psu, dh=0.53 psu, and dv=0.60 psu, respectively. The results indicate that wind direction has a large effect on retrieved SSS.

4.4 Case 4: all inputs from microwave remote sensing products

In actual practice of SMOS SSS retrieving, SST, WS, WD and τ are from other sources of database; for example, other remote sensing products, in-situ measurements, and output from the European Centre for Medium-Range Weather Forecasts (ECMWF).

If only microwave remote sensing products are used for inputs, and errors are assumed to be Gaussian, i.e., assuming ΔSST = ±1 K, ΔWS = ±1.5 m·s^{-1}, ΔWD=20°, and $\Delta\tau$=±0.0002, then we have dI=0.91 psu, dh=0.90 psu, and dv=0.93 psu, respectively.

4.5 Case 5: all inputs from all possible remote sensing products and some in-situ measurements

If all possible remote sensing products and some in-situ measurements with accuracy of ΔSST=±0.5 K, ΔWS=±1.0 m·s^{-1}, ΔWD=20°, and $\Delta\tau$=±0.0001 are used, then dI=0.61 psu, dh=0.61 psu, and dv=0.63 psu, respectively.

Table 1 summarizes the SSS errors for the five cases discussed above. It shows that if there is no error in all input parameters, RMS of the SSS will be at 0.2 psu, which is the target of SMOS mission for SSS. It is, however, impossible to have no error, since the process of SSS retrieving involves various errors in the algorithms, measurements, input data, and the true SSS for validating the retrieval. Therefore, the most likely results are those of Cases 4 and 5, which means that 0.61 psu (from Case 5) to 0.91 psu (from Case 4) may be realized by using all possible input parameters' database. Thus, global maps of SSS with RMS less than 1 psu may be quickly produced in a day. The results seem to improve the capability of SMOS in a single observation and its applications in climate models.

Tab.1 Summary of RMS of the SSS from Cases 1–5

Case	Input Parameter Noise	dI/psu	dv/psu	dh/psu
1	ΔSST=0 K, ΔWS=0 m·s^{-1}, ΔWD=0°, $\Delta\tau$=0	0.2	0.25	0.27
2	ΔSST=0 K, ΔWS=0 m·s^{-1}, ΔWD=0°, modeled τ, T_{BU} and T_{BD}	0.19	0.24	0.26
3	ΔSST=0 K, ΔWS=0 m·s^{-1}, $\Delta\tau$=0, WD=0° (no wind direction considered)	0.38	0.53	0.60
4	ΔSST=1 K, ΔWS=1.5 m·s^{-1}, ΔWD=20°, $\Delta\tau$=0.0002	0.91	0.91	0.93
5	ΔSST=0.5 K, ΔWS=1.0 m·s^{-1}, ΔWD=20°, $\Delta\tau$=0.0001	0.61	0.61	0.63

4.6 Sensitivity of SSS retrieval error to calibration biases

Here, two kinds of calibration biases are added to the simulated T_B for testing the sensitivity of the retrieved SSS to system errors. One is a constant bias for a given channel of SMOS; the other is linearly-increased biases added to their corresponding measurements.

(a) Constant bias of 1 K at all incidence angles added to the measurements of T_B

Constant calibration biases of 1K are added to the noisy T_B at all 56 incidence angles. Assuming that ΔSST=0 K, ΔWS=0 m·s^{-1}, ΔWD=0° and $\Delta\tau$=0, we find that RMS of the SSS retrieval are dI=1.80 psu, dh =2.04 psu, and dv=1.67 psu, respectively, while the standard deviations (STD) of the SSS retrieval are dI=0.33 psu, dh=0.39 psu, and dv=0.36 psu, respectively. The retrieved SSS using the Stokes I versus true SSS shows that the system biases in T_B also lead to the system biases in the SSS retrieval, but the STD in the retrieval are basically the same as in the case of no system biases (Fig.6).

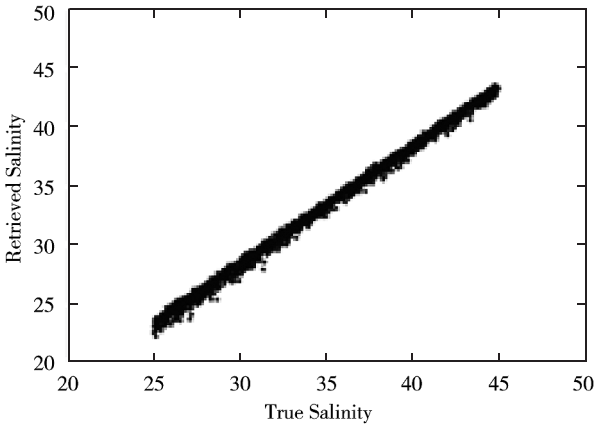

Fig.6 Retrieved SSS by Stokes I versus true SSS, with bias of 1 K at all incidence angles added to the simulated T_B

(b) Variant biases added to the measurements of T_B

A set of variant biases of T_B, say a bias of θ/55K (meaning that the added bias is θ/55K at incidence angle θ, or if θ=55°, the added error is 1K), are added to noisy T_B of 56 incidence angles, respectively. Assuming that ΔSST=0 K, ΔWS=0 m·s^{-1}, ΔWD =0° and $\Delta\tau$=0, we find that RMS of the SSS retrieval are dI =0.94 psu, dh =1.04 psu, and dv =0.97 psu, respectively, while STD of the SSS retrieval are dI= 0.23 psu, dh =0.29 psu, and dv =0.26 psu, respectively. The retrieved SSS using the Stokes I versus true SSS is shown in Fig.7.

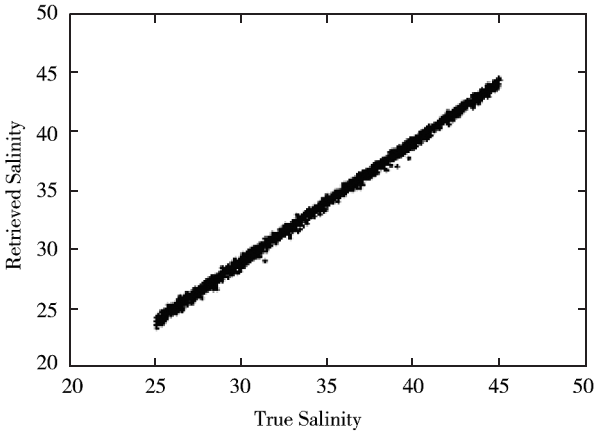

Fig.7 Retrieved SSS by Stokes I versus true SSS, with variant biases of θ/55K added to the simulated T_B at each incidence angle θ

Table 2 summarizes of Tests (a) and (b). It shows that calibration bias at all incidence angles will cause a large RMS of the SSS retrieval, but STD of the SSS retrieval are only slightly higher than that of no calibration bias in Case 1. Thus, the bias in retrieved SSS can be in advance removed in actual retrieving applications.

Tab.2 Summary of Tests (a) and (b) for RMS of SSS

Case	dI/psu	dv/psu	dh/psu
(a)	RMS=1.80	RMS=1.67	RMS=1.80
	STD=0.33	STD=0.36	STD=0.33
(b)	RMS=0.94	RMS=0.97	RMS=1.04
	STD=0.23	STD=0.26	STD=0.29

5 Summaries and implications

The MIRAS L-band radiometer has a multi-angular imaging capability, which means that each pixel is measured several times with different incidence angles due to the motion of the platform. This capability is exploited to reduce the impact of radiometric noise on salinity retrieval. A two-step algorithm is developed to inverse SSS with the help of relationship between T_B at different incidence angles. A key step of the algorithm is polynomial curve fitting of the measured noisy T_B to the incidence angles. After this step, noise embedded in measured T_B that influences SSS retrievals could be greatly reduced.

Gauss random noises of 0.2 K to 3 K, corresponding to incidence angle from 0° to 55°, are added to the simulated T_B to test the new scheme. The results of retrieving tests show that the simplified atmospheric algorithms (2)–(4) are basically accurate for SSS reversion, and wind direction has distinct effects on SSS retrievals. The results also indicate that accuracy of SSS inversed from noisy T_B may be better than 1 psu for a single overpass, even if $\Delta SST=\pm 1K$, $\Delta WS=\pm 1.5 m\cdot s^{-1}$, and $\Delta\tau=\pm 0.0002$.

From the analysis of the system biases in the calibrated T_B, a conclusion can be further drawn that calibration biases, whether a constant bias or biases linearly increasing with the incidence angles, will cause a large RMS of the SSS retrieval, but STD of the SSS retrieval is only slightly higher than that of no calibration bias. Thus, the bias in retrieved SSS can be removed in advance, and these may in turn be helpful to identify and remove calibration bias in the measurements of T_B, since the calibration bias is mostly reflected by the coefficient of p_0, a project being conducted by us right now.

References:

[1] KERR Y. The SMOS Mission (MIRAS on RAMSES): A Proposal to the Call for Earth Explorer Opportunity Mission [M]. CESBIO, Toulouse, France, 1998: 76.

[2] KERR Y H, WALDTEUFEL P, WIGNERON J P, et al. Soil moisture retrieval from space: The Soil Moisture and Ocean Salinity (SMOS) mission [J]. IEEE Trans Geosci Remote Sens, 2001, 39(8): 1 729–1 735.

[3] FONT J, LAGERLOEF G, LE VINE D, et al. The determination of surface salinity with the European SMOS space mission[J]. IEEE Trans Geosci Remote Sens, 2004, 42(10): 2 196–2 205.

[4] KOBLINSKY C, HILDEBRAND P, LE VINE D, et al. Sea surface salinity from space: Science goals and measurement approach [J]. Radio Sci, 2003, 38(4): 8064, doi: 10.1029/2001RS002584.

[5] FONT J, BOUTIN J, REUL N, et al. SMOS Sea Surface Salinity Level 2 Algorithm Theoretical Baseline Document-Issue 2[R]. European Space Agency ESTEC Contract 18933/05/NL/FF, 2007.

[6] CAMPS A, SWIFT C. New techniques in microwave radiometry for Earth remote sensing//[C] STONE W R. Review of Radio Science 1999–2002. Piscataway, NJ: IEEE Press, 2002: 499–518.

[7] ZINE S, BOUTIN J, FONT J, et al. Overview of the SMOS Sea surface salinity prototype processor [J]. IEEE Trans Geosci Remote Sens, 2008, 46(3): 621–645.

[8] CAMPS A, CORBELLA I, TORRES F, et al. The impact of antenna pattern frequency dependence in aperture synthesis microwave radiometers [J]. IEEE Trans Geosci Remote Sens, 2005, 43(10): 2 218–2 224.

[9] OBLIGIS E, BOONE C, LARNICOL G, et al. Benefits of the future sea surface salinity measurements from SMOS: Generation and characteristics of SMOS geophysical products [J]. IEEE Trans Geosci Remote Sens, 2008, 46(3): 746–753.

[10] BOUTIN J, WALDTEUFEL P, MARTIN N, et al. Surface salinity retrieved from SMOS measurements over the global ocean: Imprecisions due to sea surface roughness and temperature uncertainties [J]. J Atmos Ocean Technol, 2004, 21(9): 1 432–1 447.

[11] CAMPS A, VALL-LLOSERA M, BATRES L, et al. Retrieving sea surface salinity with multiangular L-band brightness temperatures: Improvement by spatio-temporal averaging [J]. Radio Sci, 2005, 40(2): 1–13, doi: 10.1029/2004RS003040.

[12] LIEBE H, HUFFORD G, COTTON M. Propagation modeling of moist air and suspended water/ice particles at frequencies below 1000GHz [C]//AGARD 52nd Specialists Meeting of the Electromagnetic Wave Propagation Panel. Palma de Mallorca, Spain, 1993: 3.1–3.10.

[13] SAUNDERS R. RTTOV8.5 software [CP]. EUMETSAT Satellite Application Facility on Numerical Weather Prediction (NWP SAF), 2004.

[14] CHEVALLIER F. Sampled databases of 60-level atmospheric profiles from the ECMWF analyses [R]. EUMETSAT/ECMWF SAF Program, Research Report No.4, 2001.

[15] TREGUIER A, REYNAUD T, PICHEVIN T, et al. The CLIPPER project: High resolution modeling of the Atlantic [J]. Int WOCE Newsl, 1999, 36: 3–5.

[16] PEICHL M, WITTMANN V, ANTERRIEU E, et al. Final Report: Scientific Inputs for the SMOS Level 1 Processor Development [R]. ESA contract 10508/02/NL/GS, 2005.

[17] PETITCOLIN F, BOUTIN J, VERGELY J, et al. Final Report of the Study 'Soil Moisture Retrieval for SMOS Mission', CCN2 For Sea Surface Salinity Retrieval [R]. European Space Agency ESTEC Contract 16027/02/NL/GS, SMOS-TN-ACR-LOD-006, 2005.